Check for updates

Geochemistry, Geophysics, Geosystems®

RESEARCH ARTICLE
10.1029/2026GC013098

Global Implications of Terrain-Induced Bias in Paleomagnetic Data From 3D Forward Modeling of Mt. Etna

A. E. Hendrickx[1,2], **C. Thieulot**[2], **and L. V. de Groot**[1]

[1]Paleomagnetic Laboratory Fort Hoofddijk, Faculty of Geosciences, Utrecht University, Utrecht, the Netherlands, [2]Department of Earth Sciences, Faculty of Geosciences, Utrecht University, Utrecht, the Netherlands

Key Points:

- Our Magnetic Terrain Effect (MTE) code accurately computes magnetic anomalies above highly magnetized terrain
- Large local anomalies and systematic bias can be predicted by simulating MTEs
- Terrain-induced systematic bias in lava flows is globally present and variable, and improved paleomagnetic sampling will not eliminate it

Supporting Information:

Supporting Information may be found in the online version of this article.

Correspondence to:

A. E. Hendrickx,
a.e.hendrickx@uu.nl

Citation:

Hendrickx, A. E., Thieulot, C., & de Groot, L. V. (2026). Global implications of terrain-induced bias in paleomagnetic data from 3D forward modeling of Mt. Etna. *Geochemistry, Geophysics, Geosystems*, *27*, e2026GC013098. https://doi.org/10.1029/2026GC013098

Received 2 APR 2026
Accepted 24 SEP 2026

Abstract In paleomagnetism, records of paleosecular variation (PSV) on centennial timescales are often based on magnetic measurements from lava flows. However, samples from recent flows that cooled in known magnetic fields often fail to produce the expected paleomagnetic directions, and samples from the same flow often show large within- and between-site dispersion. Direct measurements of local magnetic anomalies in volcanic terrain showed that the topography of the underlying lava flow distorts the magnetic field. Such Magnetic Terrain Effects (MTEs) are subsequently recorded by overlying flows and can account for much of this dispersion. Here we present a data-independent numerical model capable of simulating topographies and predicting magnetic fields over highly magnetized rocks. Using this Python-based forward model and high-resolution Digital Elevation Models, we replicate field measurements taken on Mt. Etna. The computed anomalies often match the location and shape of the measured results, showing intensity deviations up to 14 μT, inclination deviations up to 12°, and declination deviations up to 14°, compared to the measured deviations of 13 μT, 19°, and 21°, respectively. Our findings suggest that MTEs must be considered in paleomagnetic interpretations: while distinguishing between MTE and PSV is nearly impossible in individual measurements when the underlying topography is unknown, MTEs introduce systematic bias that can be estimated using our model. Furthermore, we demonstrate that MTE-induced bias varies globally and persists despite improved sampling strategies, necessitating the development of correction methods to address the limitations of lava flows as paleomagnetic recorders.

Plain Language Summary Paleomagnetic data from lava flows have many scientific uses, from the evolution of Earth's magnetic field and tracking past plate movement to volcanic hazard management. However, samples from recent flows that cooled in a known magnetic field often fail to produce the expected values, and even samples from the same lava flow can show large variations. Local magnetic field measurements show that the topography of the underlying lava flow can distort the magnetic field above the flow. As a result, the magnetic signal recorded by a new lava flow may be influenced by this distortion, helping to explain many of the unexpected values observed in paleomagnetic data. Here we present a computer model capable of predicting such distortions in the magnetic field above various topographies. Using topography maps of Mt. Etna, we reproduce direct measurements, producing distortions of similar size and in the same locations above certain topographic features. Extending this work beyond Mt. Etna, we show that these topography-induced anomalies are globally present and variable. Our simulations reproduce biases that have already been observed in paleomagnetic studies. Finally, we show that improved paleomagnetic sampling strategies alone cannot always eliminate these biases, highlighting the need for recognition and correction.

1. Introduction

In the study of paleomagnetism, records of paleosecular variation (PSV) are often obtained from volcanic lava flows. Volcanic rocks are recognized as good recorders of the (ancient) magnetic field due to their capacity to acquire strong and stable thermoremanent magnetizations (TRMs), capturing a magnetic vector parallel to the ambient geomagnetic field during cooling. As a result, paleomagnetic data from lava flows have a wide range of scientific uses, including constraining the chronological framework for (archeological) sites (Mahgoub et al., 2018), tracking the evolution of the Earth's magnetic field (van Grinsven et al., 2025), providing insight into tectonic evolution (Torsvik et al., 2012), and even informing volcanic hazard management strategies (Sherrod et al., 2006). Obtaining reliable absolute paleomagnetic data from lava flows is thus of eminent importance.

© 2026 The Author(s). Geochemistry, Geophysics, Geosystems published by Wiley Periodicals LLC on behalf of American Geophysical Union.
This is an open access article under the terms of the Creative Commons Attribution License, which permits use, distribution and reproduction in any medium, provided the original work is properly cited.

15252027, 2026, 10, Downloaded from https://agupubs.onlinelibrary.wiley.com/doi/10.1029/2026GC013098, Wiley Online Library on [07/11/2026]. See the Terms and Conditions (https://onlinelibrary.wiley.com/terms-and-conditions) on Wiley Online Library for rules of use; OA articles are governed by the applicable Creative Commons License

However, over the years this has proven to be surprisingly difficult as samples from the same lava flow often show large within- and between-site dispersion, exceeding the admissible error from sampling and measuring (Castro & Brown, 1987; Speranza et al., 2006). Additionally, young lava flows in for example, Italy, Hawaii, Japan, Mexico and the Canary Islands have frequently shown a magnetic vector that is inconsistent with expected International Geomagnetic Reference Field (IGRF, Alken et al., 2021) values (Coe et al., 1978; Herrero-Bervera & Valet, 2009; Meyer & de Groot, 2024; Mochizuki et al., 2004; Speranza et al., 2006; Urrutia-Fucugauchi et al., 2004; Valet & Soler, 1999). These discrepancies often require convoluted explanations to justify the interpretation of the recorded paleodirections and paleointensities. Some of these explanations include block rotations (Nyblade et al., 1987), local non-dipole geomagnetic fields (Coe et al., 1978), large-scale crustal movements (Beck, 1984), differences in field and lab cooling rates (Biggin et al., 2007; Hill & Shaw, 1999), and complex "transdomain" processes (L. V. de Groot et al., 2013). Nonetheless, most of these proposed reasons have either been discredited or have failed to fully account for the observed discrepancies (Baag et al., 1995; L. V. de Groot et al., 2013).

One proposition, the Magnetic Terrain Effect (MTE) hypothesis, suggests that irregular topography and strongly magnetized underlying rocks can locally deflect the ambient geomagnetic field, which in turn is recorded by an overlying lava flow (Baag et al., 1995; Meyer & de Groot, 2024; Speranza et al., 2006; Tanguy & Le Goff, 2004; Valet & Soler, 1999). This deflection arises from the reversed magnetic field generated by the magnetized matter below, a mechanism long recognized by those aware of magnetic compass distortions in volcanic areas. Nonetheless, MTE's significance in skewing paleomagnetic data has largely been overlooked or underestimated (Baag et al., 1995; Meyer & de Groot, 2024).

Baag et al. (1995) were the first to propose the existence of the MTE. In their study, they both modeled and measured the ambient magnetic field above different topographic features, but their 2D models could not fully reconcile the magnitude of observed inclination anomalies of up to 20° from the IGRF on Hawaii. Despite this, they established a correlation between the terrain and magnetic anomalies, a finding that has since been supported by further research, both on the Canary Islands and on Mt. Etna (Meyer & de Groot, 2024; Speranza et al., 2006; Tanguy & Le Goff, 2004; Valet & Soler, 1999). Most recently, Meyer and de Groot (2024) provided robust evidence for MTE, showing that direct magnetic field measurements above highly magnetized flows correlate with the underlying topography, with anomalies in inclination and intensity above ridges and gullies, deviating up to 19° in inclination and 20% in intensity from the IGRF. Part of the fieldwork conducted on Mt. Etna in 2018 was specifically designed to measure the magnetic anomalies above volcanic terrain with measurements taken at six sites of different lava flows on various flanks of Mt. Etna (Meyer & de Groot, 2024). These findings underscore the need to consider MTE when interpreting paleomagnetic data.

MTE poses a threat to the reliability of a paleomagnetic record for several reasons. First, since the ancient underlying terrain of a lava flow is unknown, making a distinction between dispersion due to PSV and MTE is often not possible (Baag et al., 1995). Furthermore, as MTE-induced anomalies typically extend beyond 1 m, small-area sampling and strategies aimed at minimizing data scatter are ineffective in mitigating their influence. Additionally, such strategies, when applied in rugged volcanic terrains, may inadvertently introduce systematic biases into the PSV records, which are often subtle and difficult to uncover (Meyer & de Groot, 2024; Valet & Soler, 1999).

A systematic bias in both the inclination and intensity of paleomagnetic data was identified by Meyer and de Groot (2024). On average, measurements from young Etnean lava flows were approximately 2.9° in inclination and 8.8 μT in intensity lower than predicted by IGRF values. This underestimation was possibly attributed to the MTE, particularly to the reduced ambient magnetic field within the depressions of the terrain, where new lava flows are likely to be deposited (Meyer & de Groot, 2024). Recent statistical analyses of paleomagnetic data from the past four centuries show a strikingly similar systematic underestimation of ∼3° in inclination for lava flows from the northern hemisphere (Pavón-Carrasco et al., 2016).

This evidence of systematic bias, possibly caused by MTE, highlights the need for advanced modeling techniques to predict the effects of MTE on the ambient magnetic field in volcanic regions, which is incorporated in the magnetization of volcanic rocks. In this research, we introduce a 3D, data-independent, numerical model able to simulate various topographies and compute local magnetic anomalies above volcanic terrain. The model, validated against several benchmarks, is capable of simulating a range of topographic features, from volcanic flanks to the integration of digital elevation models (DEMs), as demonstrated in simulations of Mt. Etna and the field sites from Meyer and de Groot (2024). These simulations allow us to compare the model's values to the measured

15252027, 2026, 10, Downloaded from https://agupubs.onlinelibrary.wiley.com/doi/10.1029/2026GC013098, Wiley Online Library on [07/11/2026]. See the Terms and Conditions (https://onlinelibrary.wiley.com/terms-and-conditions) on Wiley Online Library for rules of use; OA articles are governed by the applicable Creative Commons License

anomalies in the field, investigate their origins, and determine the terrain shapes most capable of producing them. Moreover, as these anomalies are embedded into any subsequent solidifying flow, modeling them provides an opportunity to study the incorporation methods within any future layers on top of today's topography. This paves the way for possible removal of MTEs from future paleomagnetic records. Lastly, the model can be used to enhance the accuracy of global paleomagnetic models by estimating adequate scatter for similar research areas. In this study, apart from presenting this MTE code, we will focus on using the MTE code to investigate terrain-induced bias in paleomagnetic data, as suggested by Meyer and de Groot (2024) on Mt. Etna, and extend our insights to the global field of paleomagnetic research.

2. Methods

Understanding how volcanic topography modifies the ambient magnetic field requires a clear description of the underlying physics. We therefore begin by deriving the governing equations that link the thermoremanent magnetization of volcanic rocks to the magnetic anomalies measured above the surface. This formulation provides the foundation for the computational approach and model configurations described in the following sections.

2.1. Governing Equations

Our aim is to compute the magnetic field generated by magnetized matter, in the presence of the Earth's magnetic field and outside the source, that is, above the Earth's surface. The anomalous field is produced by the magnetized volcanic rock. As the rock cools, certain minerals become magnetic, and their dipole moments align with the ambient magnetic field; upon further cooling, they retain this alignment as a TRM (Tauxe, 2010). Considering these minerals as tiny dipoles at a sufficient distance (i.e., outside the source), the material's magnetization $\mathbf{M}$ is equal to its magnetic dipole moment $\mathbf{m}$ per unit volume V (Reitz & Milford, 1967). This relationship allows for the magnetic field of a dipole $\left(\mathbf{B}_{dip}(\mathbf{r}) = \frac{\mu_0}{4\pi}\left[\frac{3\mathbf{r}(\mathbf{m}\cdot\mathbf{r})}{r^5} - \frac{\mathbf{m}}{r^3}\right]\right)$ to be expressed as an integral over the magnetized volume (Griffiths, 2013). We assume a uniform magnetization across the volcanic flow, which allows for the reduction of the volume integral to a surface integral. At any given point $\mathbf{r}$, the total magnetic field $\mathbf{B}_t(\mathbf{r})$ comprises the Earth's (assumed) uniform magnetic field $\mathbf{B}_0$ and the anomalous field, leading to the fundamental equation:

$$\mathbf{B}_t(\mathbf{r}) = \mathbf{B}_0 + \frac{\mu_0}{4\pi}\oint_S \frac{(\mathbf{M}(\mathbf{r}')\cdot\hat{\mathbf{n}})\,(\mathbf{r}-\mathbf{r}')}{|\mathbf{r}-\mathbf{r}'|^3} ds' \tag{1}$$

This equation reflects the magnetized body's surface contribution to the total magnetic field, where $\hat{\mathbf{n}}$ is the unit vector normal to the surface S, μ_0 is the permeability of free space, $\mathbf{r}$ is the observation point position vector, $\mathbf{r}'$ is the position vector of a source point on the surface of the magnetized body, and $|\mathbf{r}-\mathbf{r}'|$ is the distance between the observation point and an element with surface ds' (Figure 1). For a full derivation of this equation, see the documentation of the code (Hendrickx & Thieulot, 2026). To simplify, the total magnetic field is equal to the reference field added to the magnetic field produced by the magnetized matter, and the latter is the sum of contributions of the magnetic moments of all elements inside the volume.

2.2. Computational Approach

In the previous section, we have established that the anomalous field can be computed by summing the magnetic contributions of each element within a volume. This is implemented in our code using a 3D polyhedral forward model to evaluate the surface-integral formulation. First, a 3D model domain is generated with the required topography for simulations, which is consequently discretized into a mesh of elements with uniform magnetization. In the simulations presented here, we prescribe a constant magnetization in the underlying flow and ignore any spatial variation in the magnetization due to mineralogy, self-demagnetization, or induced magnetization. This is not to imply that the influence of such variations is insignificant; their effects have been investigated and deemed substantial in other studies (Knudsen et al., 2003). However, in this study we focus solely on the influence of the topographical variations of the underlying flow on the magnetic field above its surface.

15252027, 2026, 10, Downloaded from https://agupubs.onlinelibrary.wiley.com/doi/10.1029/2026GC013098, Wiley Online Library on [07/11/2026]. See the Terms and Conditions (https://onlinelibrary.wiley.com/terms-and-conditions) on Wiley Online Library for rules of use; OA articles are governed by the applicable Creative Commons License

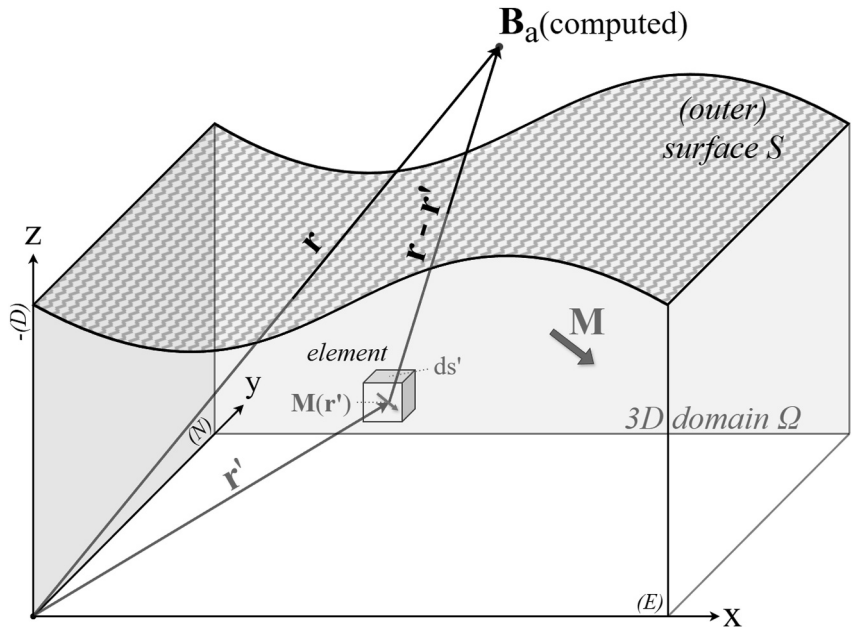


Figure 1. At any given position **r** the resulting magnetic field **B** is the sum of the contribution from all elements in the object Ω.

The magnetic anomaly at an observation point **P** is computed by solving the surface integral, the second part of Equation 1, for each element within the model domain. This method, rooted in the works of Bott (1963), projects the magnetic effects of each element's face onto triangles and evaluates their influence based on proximity to **P** (Blakely, 1995). After assigning topographical values to the corner nodes of an element's top surface, nodes may not reside in a singular plane. This requires each element's top and bottom surfaces to be subdivided into four additional triangles for a total of 12 faces and 10 nodes defining an element. Several spatial problems due to singularities of this method are mitigated by applying a small ($<10^{-5}$ m) offset to the location of observation points that coincide with a cell edge or diagonal of the top surface, allowing for computation (additional information is provided in the code documentation, Hendrickx & Thieulot, 2026). By adding contributions from each cell, the cumulative magnetic effect of the model domain is computed, as illustrated in Figure 1. Next, these magnetic field components are added to the Earth's reference field to determine the total components of the magnetic field.

A key assumption vital to this computational approach is that the mesh elements are sufficiently small and their distance to **P** is large enough. This may be problematic, especially for those elements nearest to the observation point. According to Jackson (1999), distance-related errors are trivial unless **P** lies within a few molecular diameters of a uniformly magnetized element. This suggestion is supported by empirical evidence from similar studies (Baag et al., 1995), affirming the model's validity for the paleomagnetic applications in this study.

Additionally, the computational approach and each underlying assumption have been validated through four distinct benchmarks detailed in the code's documentation (Hendrickx & Thieulot, 2026). These benchmarks include comparisons with both analytical solutions and the numerical results of Ren et al. (2017, 2019), the results of which are included in Text S1, Figures S1, and S2 in Supporting Information S1. The maximum deviation observed from the established benchmark is a mere 0.1 μT, demonstrating the code's accuracy, particularly in simulations at close proximity to uniformly magnetized bodies.

2.3. Model Setup

This section presents the model configurations used for flank simulations and reproducing direct field measurements. To validate the results of these models, the impact of various setup parameters and initial boundary conditions has been investigated for both synthetic topography models and those derived from DEM. Some of

15252027, 2026, 10, Downloaded from https://agupubs.onlinelibrary.wiley.com/doi/10.1029/2026GC013098, Wiley Online Library on [07/11/2026]. See the Terms and Conditions (https://onlinelibrary.wiley.com/terms-and-conditions) on Wiley Online Library for rules of use; OA articles are governed by the applicable Creative Commons License

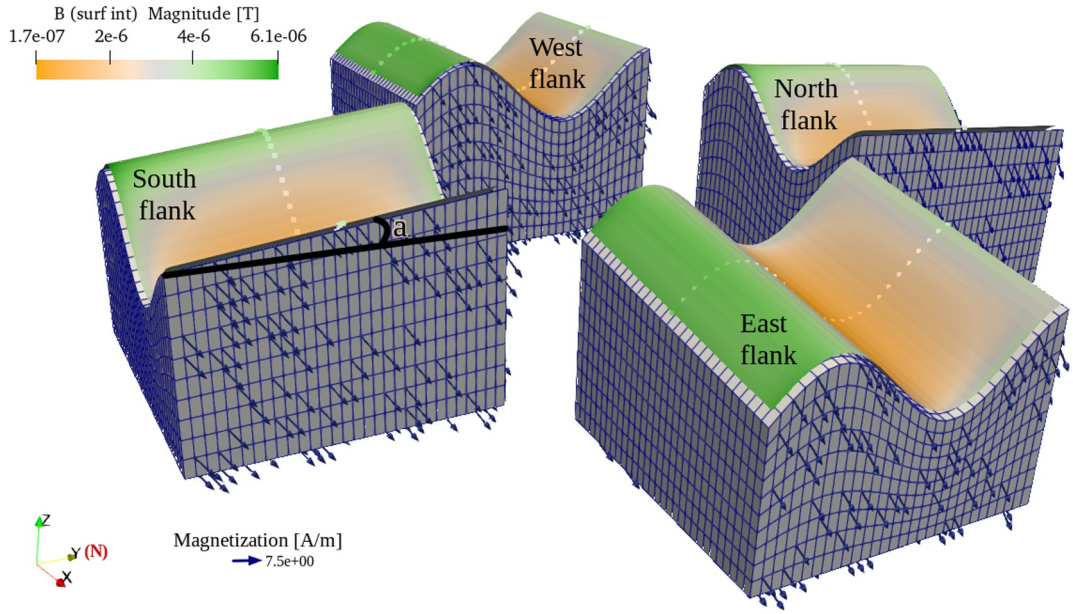


Figure 2. Visualization of the model setup of a flank simulation on Mt. Etna using $\mathbf{M} = 7.5\ A/m$ (arrows), and a slope (a) of 6°, displaying both the model domain and measurement paths. For visual clarity, the extent and resolution of the displayed model domain do not adhere to the optimized testing setup outlined in the text.

these parameter choices will be reviewed in the discussion, and a full detailed rationale can be found in the code documentation (Hendrickx & Thieulot, 2026).

All model setups, both synthetic and DEM-derived models, feature a flat bottom surface at 20 m below the minimum surface elevation. This ensures that the spatial extent of the model domain greatly exceeds the depth extent, which has been verified to improve model accuracy during parameter testing and aligns with recommendations of Bott (1963). Additionally, to eliminate any effect of varying model domain size and focus specifically on the influence of surface topography, the data from the topographic models are calibrated against those from a flat-terrain model of equivalent dimensions.

2.3.1. Synthetic Topography: Flank Simulations

Given that the majority of lava flows are located on the flanks of volcanoes, simulating volcanic flanks is a relevant starting point for our generic modeling setup, allowing broad flank-specific trends to be isolated. It is expected that each flank produces different anomalies due to the variation in the dip direction of the surfaces, while the magnetization direction remains consistent in the magnetized matter below. On Mt. Etna, the typical lava flow morphology is characterized by ridges and gullies. These features are replicated in our model setup using a sine function traversing perpendicularly across an inclined surface. The model allows for manipulation of several parameters: the slope of the surface, the amplitude and wavelength of the sine function, and the orientation of the sine wave's propagation relative to the Cartesian axes, see Figure 2.

For alignment with the case study, the parameters used to define the synthetic topography were chosen to replicate the ridges and gullies of Mt. Etna. Based on the analysis of aerial imagery and DEMs of the area around the field sites of Meyer and de Groot (2024), an amplitude of 4 m, a wavelength of 25 m, and an angle of inclination for the slope of 6° were found to be representative values. A uniform remanent magnetization intensity of 7.5 A m^{-1} was assigned to the simulated matter. This value aligns closely with the average TRMs measured in lava flow samples from the field, as reported in Meyer and de Groot (2024), and with the magnetization intensities found in prior paleomagnetic research on Etnean lavas by Nicolosi et al. (2014), which documented a bulk magnetization of 8 A m^{-1} and a range between 5 and 13 A m^{-1}. However, it is worth noting the broader spectrum of recorded values in other studies, from as low as $0.1 - 1$ A m^{-1} to as high as 20 A m^{-1} (Speranza et al., 2006; Tanguy & Le Goff, 2004), indicating the significant variability in magnetization measurements of Etnean lavas. Directional paleomagnetic data from Mt. Etna are similarly variable and frequently deviate from the expected field direction

15252027, 2026, 10, Downloaded from https://agupubs.onlinelibrary.wiley.com/doi/10.1029/2026GC013098, Wiley Online Library on [07/11/2026]. See the Terms and Conditions (https://onlinelibrary.wiley.com/terms-and-conditions) on Wiley Online Library for rules of use; OA articles are governed by the applicable Creative Commons License

(Meyer & de Groot, 2024). We therefore assume a geocentric axial dipole (GAD) to compute the direction of the magnetization in the underlying material instead of relying on paleomagnetic measurements. At Mt. Etna's latitude, this gives a magnetization inclination of 57° and a declination of 0°. The reference magnetic field in the flank simulations was calibrated to the average of the IGRF-13 values of Etna's flanks (Alken et al., 2021), with the respective components being $IGRF_E = 1561.2$ nT, $IGRF_N = 26850.3$ nT, and $IGRF_D = 36305.7$ nT.

Flank simulations were done using a model domain of 250 × 250 × 20 m discretized with 375 × 375 × 10 elements. Computations were conducted along a path comprising 47 points positioned 1 and 1.8 m above the middle of the model domain, with observation points distributed at approximately 1 m intervals.

2.3.2. DEM Topography and Field Paths

To reproduce the FLUX field sites of Meyer and de Groot (2024), two DEMs of Mt. Etna and the surrounding regions were incorporated into the MTE code. A map of the locations of the FLUX sites with the ages of the lava flows is shown in Figure S3 in Supporting Information S1. Before computation of the magnetic field values above the surface, the 2 × 2 m resolution DEM Siciliana (2010), geo-referenced in ROMA 40/EST - EPSG 3004 using the Gauss–Boaga projection, has been converted to WGS84 UTM 33N in ArcGIS Pro through bilinear interpolation. This 2 m DEM, available on the SITR web platform, did not list specific data acquisition details. The 5 × 5 m spatial resolution DEM (Bisson et al., 2016) utilizes the WGS84 UTM 33N System and is noted for its vertical accuracy with a root-mean-square error of ±0.24 m. Both DEMs were derived from airborne LiDAR. The 5 m DEM is a resampled version of a 2 m DEM (Bisson et al., 2016), and while the original data's vertical and horizontal accuracy was preserved, using a 5 m DEM inherently limits us to a 5 m resolution, thereby capping our accuracy. Unfortunately, the original 2 m DEM was not publicly available, necessitating the use of the 5 m DEM in this study.

In the parameter experiments documented in the code's manual (Hendrickx & Thieulot, 2026), it was determined that a recommended minimum spatial extent of 250 × 250 m is necessary for paths approximately 50 m in length to avoid any edge effect at the observation points. Most of the FLUX paths are between 50 − 70 m (Meyer & de Groot, 2024); consequently, the DEM cutouts used for generating our final results were approximately 300 × 300 m for most sites and paths. For specific dimensions of these cuts at each site, see Table S1 in Supporting Information S1. The depth of the model is discretized with 10 elements across all sites, while the spatial element resolution varied according to the specific DEM selected for each location. In the initial stages of testing, we conducted experiments with multiple model domain sizes, and these tests revealed only minor discrepancies between various model domain sizes, as illustrated in Figure S4 in Supporting Information S1.

For the replication of direct measurements, a path was generated from the GPS coordinates of the field data, using the x & y coordinates from the field path, and fixing the height at a constant value above the DEM surface. The GPS field data were converted from decimal degrees to WGS84 UTM 33N, and calibrated to align with the DEMs. Additionally, the height of the GPS device, set 2 m above ground level (B. M. de Groot & de Groot, 2019), was accounted for in the field data processing.

3. Results

3.1. Flank Simulations

In Figure 3 the results of the flank simulations done for Mt. Etna are presented, where each flank reveals a unique pattern. The maximum intensity anomalies observed relative to Mt. Etna's IGRF intensity, across all simulated topographies of the volcano's flanks, are approximately +2.6 μT for positive anomalies and −2.83 μT for negative anomalies, both observed on the west flank. The largest inclination anomaly peaks at about +3.07° in the positive spectrum on the east flank and −4.39° in the negative on the west flank. Similarly, the largest declination anomaly is +4.98° for positive deviations and −5.14° for negative deviations, both observed on the southern flank.

A striking observation is the contrasting shapes of the intensity and inclination deviations for both the positive and negative ranges across all flanks. Positive deviations in intensity and inclination are generally confined to narrower regions around the gullies and ridges, whereas negative deviations appear broader and stretch further from the topographic landmarks. This can also be seen if we look at the average median difference with respect to the IGRF for all flanks, where the inclination and intensity medians lie below the IGRF, with an average difference of

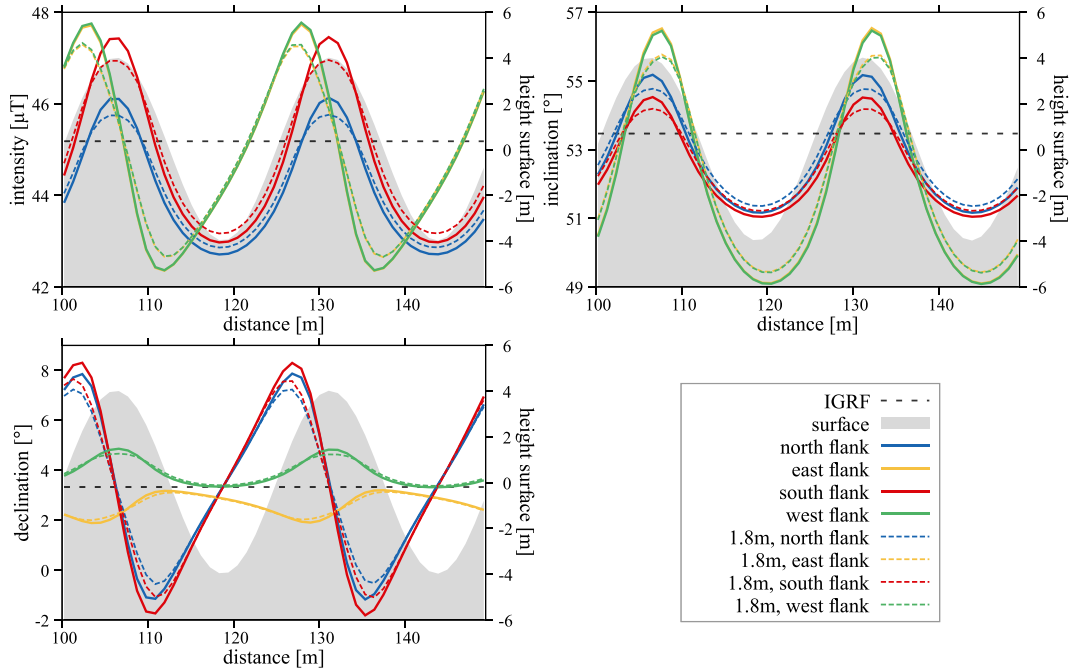


Figure 3. The intensity [μT], inclination [°] and declination [°] of the computed magnetic field **B** derived from simulated flanks, where negative anomalies extend over a broader region compared to positive anomalies.

−0.91 μT for intensity, −1.77° for inclination, and −0.02° for declination (see Table S2 in Supporting Information S1).

When comparing the alignment of anomalies with respect to the topography, we observe spatial offsets between the peak of magnetic anomalies and the peak in topography for certain flanks. For the east and west flanks, peaks in intensity appear further south (to the left in Figure 3) and peaks in inclination appear further north (to the right in Figure 3) relative to their north-south counterparts and the topography. This misalignment is most pronounced for the south and north flanks' declination values, where anomaly highs are located roughly 5 m west of the topographical peak (to the left in Figure 3).

At first glance, the curves computed at a higher altitude seem consistent with the observations at lower altitudes (Figure 3). The strength of the anomaly decreases with altitude, aligning with magnetic principles where magnetic field variations diminish in intensity as the distance from their source increases (Reitz & Milford, 1967). However, negative anomalies in intensity and inclination display greater persistence at elevated altitudes, exhibiting a less pronounced reduction in magnitude with height than the positive anomalies above ridges, showing the complex interplay between topographic influence and the geomagnetic field.

3.2. DEM Derived Models

3.2.1. Matching the FLUX Sites With DEMs

The DEMs and corresponding measurement paths used in this study are based on the FLUX site locations and path configurations presented by Meyer and de Groot (2024). Two DEMs were available: one with a spatial resolution of 2 m (Siciliana, 2010) and another one with 5 m (Bisson et al., 2016). Although the 2 m DEM was expected to provide greater detail than the 5 m DEM, the available 2 m DEM's performance proved inconsistent across the study area. The 2 m DEM unfortunately lacked precision across many locations, with topographies of most flows excessively smoothed, and some areas appearing entirely flat. By contrast, the 5 m DEM generally provided a credible match with the topography for most paths across all sites except FLUX3, as it was located outside the region covered by the 5 m DEM. Hence, for all other sites apart from FLUX3, the 5 m DEM served as the primary source for subsequent tests. See Figures S5–S11 in Supporting Information S1 for visual depictions of the 2 and 5 m DEMs at all the FLUX sites.

15252027, 2026, 10, Downloaded from https://agupubs.onlinelibrary.wiley.com/doi/10.1029/2026GC013098, Wiley Online Library on [07/11/2026]. See the Terms and Conditions (https://onlinelibrary.wiley.com/terms-and-conditions) on Wiley Online Library for rules of use; OA articles are governed by the applicable Creative Commons License

15252027, 2026, 10, Downloaded from https://agupubs.onlinelibrary.wiley.com/doi/10.1029/2026GC013098, Wiley Online Library on [07/11/2026]. See the Terms and Conditions (https://onlinelibrary.wiley.com/terms-and-conditions) on Wiley Online Library for rules of use; OA articles are governed by the applicable Creative Commons License

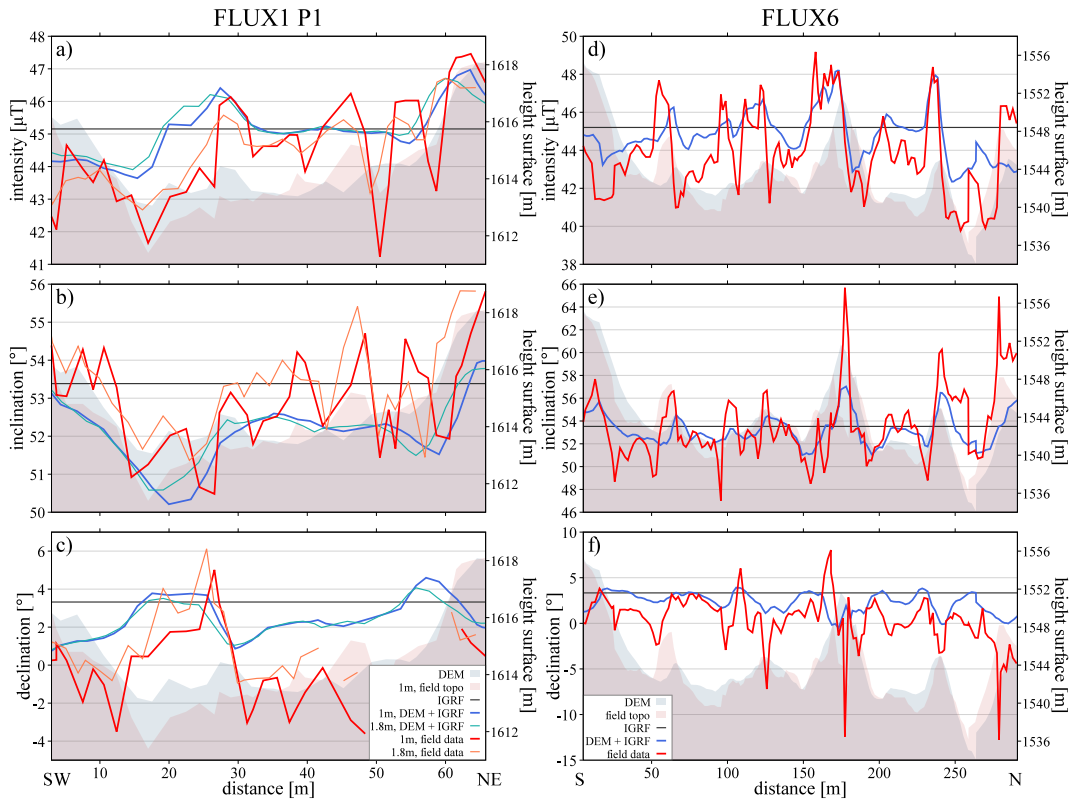


Figure 4. (a, d) Intensity, (b, e) inclination, and (c, f) declination results from both direct measurements (field data) and model values (DEM + IGRF) for (a–c) FLUX1, path 1, and (d–f) FLUX6. The results are plotted together with the DEM topography and topography measured in the field and the expected IGRF at each site in 2018. If the DEM topography coincides with the field topography, the computed and measured anomalies are similar in shape, size and general location.

In the case of paths 1 and 2 at FLUX4, a glaring discrepancy was observed between the field-measured topography and both DEMs. Meyer and de Groot (2024)'s notes indicated a GPS malfunction between measuring path 1 and path 2, with errors only in the lowest height measurements of these paths. However, our analysis indicates that the GPS data for all heights at these paths were unreliable. As a result, we have excluded these paths from further analysis.

Across other sites and paths, the data set of Meyer and de Groot (2024) also had missing declination measurements at points where the irregular terrain obstructed their view of the reference point. Most sites show a height offset between the DEM and direct GPS measurements. This offset was calculated as the difference between the mean field-measured heights and the DEM height at the corresponding *xy*-coordinates. In some instances, minor spatial misalignment was also detected and corrected based on topographic visualizations. To ensure accurate comparisons, these offsets were subtracted from the original data prior to plotting. For specific offset values, please see Table S1 in Supporting Information S1.

As shown in Figure 4, even the 5 m DEM, while generally more reliable, exhibited a tendency to smooth the landscape. This resulted in fewer, less distinct peaks and troughs, and a softening of sharp topographical transitions.

3.2.2. Reproducing Direct Measurements With DEMs

This section highlights key findings and potential insights for FLUX1 and FLUX6, although similar observations are consistent across most paths and sites. The results for all sites and paths are detailed in Figures S12–S23 in Supporting Information S1.

A significant observation from FLUX1 path 1 (Figures 4a–4c) is that agreement between DEM topography and field-measured topography corresponds to improved agreement between computed and measured magnetic field

15252027, 2026, 10, Downloaded from https://agupubs.onlinelibrary.wiley.com/doi/10.1029/2026GC013098, Wiley Online Library on [07/11/2026]. See the Terms and Conditions (https://onlinelibrary.wiley.com/terms-and-conditions) on Wiley Online Library for rules of use; OA articles are governed by the applicable Creative Commons License

Table 1
Intensity (int) [μT], Inclination (inc) [°], Declination (dec) [°], Standard Deviation (σ), Minimum (min), Maximum (max), and Median Difference w.r.t. the IGRF ($\widetilde{\Delta}$) for the Model, Direct Measurements (Field), and IGRF Values of FLUX6

FLUX6	Field	IGRF	Model-1	Model-2
Int $\pm\sigma$	43.61 ± 2.19	45.20	44.75 ± 1.31	44.20 ± 2.49
Min	39.77		42.35	38.72
Max	49.18		48.23	52.31
$\widetilde{\Delta}$	−1.59		−0.45	−1.00
Inc $\pm\sigma$	53.04 ± 3.09	53.53	52.95 ± 1.35	52.64 ± 2.62
Min	47.02		51.01	48.45
Max	65.69		57.03	60.20
$\widetilde{\Delta}$	−0.48		−0.58	−0.89
Dec $\pm\sigma$	0.71 ± 2.76	3.33	2.41 ± 1.14	1.64 ± 2.40
Min	−12.75		−0.53	−5.46
Max	8.03		3.92	8.73
$\widetilde{\Delta}$	−2.62		−0.93	−1.69

Note. Model-1 uses a magnetization of 7.5 A m^{-1}. Model-2 increases the magnetization strength to 13 A m^{-1} and includes DEM noise of −1.5 to 1.5 m.

anomalies of Meyer and de Groot (2024). At this site, the larger topographical features are well represented in both DEM and direct measurements, producing a similar overall trend for the model and measured anomalies. However, the 5 m DEM's finer topography does not align with the direct measurements in the mid-section of the path (approximately 25 − 55 m), causing misalignment between computed and measured data and a reduced expression of anomalies over the terrain. Almost all mismatches between computed and measured values occur in regions where differences between field and DEM topography are also apparent. This pattern is likewise evident at FLUX6 (Figures 4d–4f), where a close match between the 5 m DEM and field topography results in better agreement between computed values and measured anomalies.

Table 1 outlines the range of deviations for both computed values and direct measurements, and the median difference to the IGRF for FLUX6. The computed values show intensity deviations of 6 μT, inclination deviations up to 6° and declination deviations up to 4° (for model-1). The measured deviations in the field were intensity deviations of at most 9 μT, inclination deviations up to 19° and declination deviations up to 21° (Table 1) (Meyer & de Groot, 2024). For all other sites, these statistical measures are included in Tables S3–S9 in Supporting Information S1. General observations for the computed values at sites well-represented by a DEM include:

1. The intensity variations correlate with the underlying topography: they increase in magnitude above ridges in the topography, and decrease in valleys. This matches the trends in the direct measurements. The median intensity of the direct measurements shows negative anomalies relative to the IGRF at all sites. In contrast, the computed median intensity only shows such negative anomalies at FLUX1, FLUX3 and FLUX6 (see Tables S5 and S6 in Supporting Information S1). The computed intensity values do not fully cover the entire range of the deviations in direct measurements for all sites, averaging only 60% of the full extent of the anomalies in the direct measurements.
2. The inclination correlates with the underlying topography, with a similar trend as the intensity. Peaks and dips in computed inclination generally align with the direct measurements for similar topographies. The median computed inclination matches the direct measurements well, with no significant offset. Both the direct measurements and the computed values are typically 1 − 2° lower than IGRF expectations (see Tables S5 and S6 in Supporting Information S1). Again, standard deviations, the minimum, and maximum values of the computed values show less deviation from the IGRF than those of the direct measurements.
3. The declination shows significant deviations from the median values of the direct measurements, whereas the computed values display less pronounced deviations. Trend matching is challenging, often due to missing declination data for the direct measurements. However, both the computed and direct measurement values are lower than the values predicted by the IGRF.

15252027, 2026, 10, Downloaded from https://agupubs.onlinelibrary.wiley.com/doi/10.1029/2026GC013098, Wiley Online Library on [07/11/2026]. See the Terms and Conditions (https://onlinelibrary.wiley.com/terms-and-conditions) on Wiley Online Library for rules of use; OA articles are governed by the applicable Creative Commons License

In summary, the computed trends tend to be smoother and exhibit less pronounced deviations, as supported by statistical parameters of the data in Tables S3 and S4 in Supporting Information S1, showing lower standard deviations in computed values compared to the direct measurements.

Across all paths, sites, and simulations, there is a notable increase in induced anomalies near the surface, evident in both the direct measurements and computational predictions. This is confirmed by comparing standard deviations of both computed data and direct measurements at different heights (Tables S3 and S4 in Supporting Information S1), with lower deviations at 1.8 m compared to 1 m for all sites.

4. Discussion

4.1. Comparing Direct Measurements and Model Results

To assess the role of topography in shaping magnetic anomalies, we compare the direct measurements with computed values derived from our DEM-based model. Both data sets show a clear and consistent pattern: magnetic anomalies are strongly governed by changes in topography. In areas where the DEM accurately reproduces field topography, the computed and measured anomalies closely match in shape, magnitude and location. Where discrepancies exist between the DEM and the field topography, both data sets still produce internally consistent anomalies that reflect their respective surface forms. Flat terrain, as in the DEM along FLUX5 path 1 (Figure S21 in Supporting Information S1), yields no discernible anomalies, highlighting the dependence of magnetic variations on local relief.

A consistent difference between the direct measurements and computed predictions is that the modeled anomalies are generally less pronounced. They display fewer peaks and smaller deviations in inclination and declination, as evident from the minimum and maximum values for FLUX6 (Table 1). This attenuation is likely due to the inherent limitations of DEMs in capturing the ruggedness of volcanic terrain, leading to a smoothing effect that diminishes the extremities in magnetic data.

To assess how this inherent smoothing in the DEMs influences the results, we added random noise to the DEMs following the approach of Tate et al. (2005). Random perturbations of −2 to 2 m were applied to the top surface midpoints of our model's elements, while the corner nodes retained the original DEM elevation values. Introducing such variability increased the intensity deviations to as much as 12 μT, and inclination and declination deviations up to 9°. Given that Mt. Etna's lava flows are predominantly aa-type, characterized by rugged terrain with debris ranging from small stones to large boulders (Kilburn & Lopes, 1988; Meyer & de Groot, 2024), adding up to 2 m noise aligns with realistic topographical variations. The inclusion of noise notably increased the number and amplitude of anomalies, yielding a closer match to the abrupt magnetic field variations seen in the direct measurements (Figures S24 and S25 in Supporting Information S1). However, when noise amplitudes reached ±2 m, some intensity anomalies became larger than those observed in the direct measurements. Since intensity deviations of up to 13 μT occur at other FLUX sites, these values remain plausible. Even so, the inclination and declination deviations still did not fully reproduce the larger excursions seen in the direct measurements, which reach up to 19° and 21°, respectively.

Another factor potentially leading to discrepancies between the direct measurements and the model results is the uniform magnetization assigned to the lava flows in the simulations. The magnetization of 7.5 A m^{-1} used for our models is typical for Etnean lavas, yet not universally applicable to all lava flows on Mt. Etna (L. V. de Groot et al., 2013; Meyer & de Groot, 2024; Nicolosi et al., 2014; Speranza et al., 2006; Tanguy & Le Goff, 2004). As illustrated in Figures S26 and S27 in Supporting Information S1, increasing the magnetization amplifies both the frequency and magnitude of the intensity, inclination, and declination anomalies, whereas reducing it has the opposite effect. For instance, applying a magnetization of 20 A m^{-1}, as suggested by Speranza et al. (2006), resulted in intensity deviations up to 16 μT, and inclination and declination deviations of up to 16° and 12°, respectively. With this magnetization, the inclination matches the full range of anomalies as observed in the direct measurements, whereas the intensity anomalies exceed those measured in the direct measurements, and the declination still does not match the largest peaks.

Combining adjustments to the magnetizations and the introduction of noise into the DEM substantially improved the agreement between modeled magnetic field predictions and direct measurements for FLUX6, as showcased in Figure 5 and Table 1. The computed intensity deviations reach up to 14 μT, inclination deviations up to 12°, and

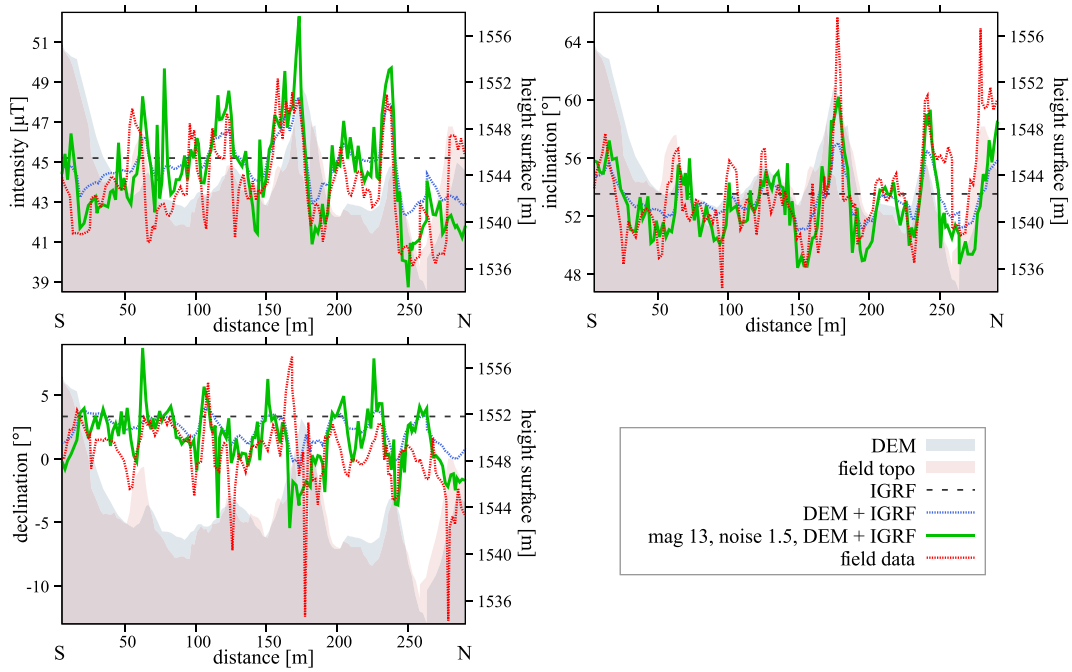


Figure 5. FLUX6 results with model-2 setup, increased magnetization of 13 A m^{-1} and a DEM with noise between −1.5 and 1.5 m, showing an improved match of direct measurements (field) and model values.

declination deviations up to 14°. Despite these improvements, the full range of inclination and declination deviations observed in the direct measurements is not entirely reproduced. The most extreme deviations in the direct measurements occur near a distinct topographic feature resembling a crack around 175 m along the profile of FLUX6. Baag et al. (1995) demonstrated that such sharp features can significantly amplify inclination anomalies beyond what is typically seen with most other forms of relief. Crucially, features of this type are rarely resolved in DEMs or created by noise application, emphasizing the need to include common volcanic features in future MTE model studies to better reproduce their effects.

It is also important to consider the accuracy of the direct measurements. Meyer and de Groot (2024) obtained paleomagnetic directions using a magnetic compass due to weather conditions, which can introduce large declination offsets due to differences between the Sun and magnetic compass readings for Mt. Etna (Speranza et al., 2006). This could explain some of the unusually large declination variations in the direct measurements.

In addition, our model assumes a homogeneous magnetization throughout the lava flow, ignoring potential variations in mineral distribution or concentration and effects of self-demagnetization and induced magnetization in the magnetized body. Knudsen et al. (2003) reported that these effects can cause internal deflections of up to 6° within a single flow. Considering our model's zero-declination assumption and the small declination of the IGRF in this region, such local deviations could significantly affect declination values. The validity of neglecting induced magnetization and self-demagnetization depends on the ratio of remanent to induced magnetization in the underlying rock, known as the Koenigsberger ratio. For Etnean lava flows, this ratio is typically high ($5 - 10$) (Branca et al., 2019; Del Negro & Ferrucci, 1998; Magli et al., 2024), supporting our assumption. Nevertheless, this assumption may be less appropriate in volcanic settings where this ratio is low. Ren et al. (2022) recently developed analytical expressions to describe magnetic fields produced by 3D polyhedra with spatially varying magnetization vectors. Different magnetizations can already be prescribed to individual elements in our model, allowing cell-based spatial variations. Incorporating these equations into the MTE code would allow future studies to account explicitly for heterogeneous magnetizations within individual elements and improve model predictions. At the same time, the exact distribution of the magnetization within a single flow is rarely known, so the feasibility of incorporating these variations in model simulations remains to be tested.

An enhanced DEM resolution would further improve the accuracy of our simulations. In the present data set, a single DEM height point represents approximately five direct measurement points, meaning that small-scale

15252027, 2026, 10, Downloaded from https://agupubs.onlinelibrary.wiley.com/doi/10.1029/2026GC013098, Wiley Online Library on [07/11/2026]. See the Terms and Conditions (https://onlinelibrary.wiley.com/terms-and-conditions) on Wiley Online Library for rules of use; OA articles are governed by the applicable Creative Commons License

15252027, 2026, 10, Downloaded from https://agupubs.onlinelibrary.wiley.com/doi/10.1029/2026GC013098, Wiley Online Library on [07/11/2026]. See the Terms and Conditions (https://onlinelibrary.wiley.com/terms-and-conditions) on Wiley Online Library for rules of use; OA articles are governed by the applicable Creative Commons License

topographic details recorded in the direct measurements cannot be fully expressed in the model predictions. The relatively strong agreement between the computed anomalies and direct measurements achieved at FLUX6 likely results from the longer path length and longer distances between measurement points, which emphasize larger scale topographical variations that are better resolved by the DEM.

A final factor potentially contributing to remaining discrepancies between the direct measurements and model predictions is the addition of the reference field (IGRF) to the computed data. Although recent studies confirm the IGRF's reliability in Italy (Di Mauro et al., 2021), minor local deviations could still influence the results. Incorporating spatial and temporal variations of the reference magnetic field into the MTE code would therefore be a valuable direction for future development.

4.2. Flank Simulations and Systematic Bias

For all FLUX sites, direct measurements and modeled values show persistent lower values for the median intensity, inclination, and declination when compared to the expected IGRF values (Table 1 for site FLUX6). In this section these discrepancies are compared to the flank simulation results, where the observed trends can be used to explain and generalize most findings and characterize the resulting systematic bias.

Gullies and ridges on the flanks of Mt. Etna produce large, laterally extensive, and persistent negative anomalies in both intensity and inclination that extend well beyond the width of individual depressions, see Figure 3. Our simulations show that these systematic negative anomalies naturally arise from the geometry of the terrain itself and explain the inclination shallowing and reduced intensities documented by Meyer and de Groot (2024). This does not even require localized deposition in the topographic lows, as proposed by Meyer and de Groot (2024) as an explanation for the bias: if all flanks were fully covered by a new layer of lava, this flow would, on average, still have a more shallow and less intense magnetization than the IGRF. Additionally, as this inclination shallowing due to rugged volcanic topography is expected to be present throughout the northern hemisphere, inclusion of MTE into lava flow records also provides an explanation for the systematic $\sim 3°$ inclination underestimation reported for the northern hemisphere by Pavón-Carrasco et al. (2016).

Furthermore, the declination patterns predicted by our flank simulations shed light on the MTE-related trends observed in the direct measurements. FLUX3, FLUX4, and FLUX6 (Figure 4 and Table 1; Table S5 in Supporting Information S1), all located on the east flank (see Figure S3 in Supporting Information S1), exhibit the strongest negative median declination differences. These values agree with our flank simulations, which predict only negative declination anomalies on this side of the volcano (Figure 2 and Table S2 in Supporting Information S1). This observation indicates that a systematic declination bias can emerge when sampling is geographically restricted to specific flanks. This pattern is also reflected in Meyer and de Groot (2024)'s study, where most sampling sites were located on either the south, north-eastern or eastern flank, yielding a median declination 6.5° lower than the IGRF values at the time of the eruption. Meyer and de Groot (2024) noted that this bias was difficult to reconcile with the absence of a systematic declination offset in the full data set of paleomagnetic studies of historical lava flows on Mt. Etna. This discrepancy, however, is actually consistent with our flank simulations: the combined paleomagnetic data set includes several additional sites on the western side of the volcano, where declination anomalies are predicted to be predominantly positive, effectively canceling the observed east-flank bias. Together, these results emphasize that avoiding MTE-related declination bias in rugged volcanic terrain requires sampling lava flows from all sides of a volcano, ensuring that positive and negative declination anomalies are balanced.

The "misaligned" peaks in the magnetic data with respect to the topographic features, as first described by Meyer and de Groot (2024), can also be clarified by comparing our MTE model results, the direct measurements, and flank simulations. At FLUX6 (east flank), the simulation, model, and direct measurements consistently show an intensity peak located south of the topographical high (Figures 6a and 6d) and an inclination peak located further north than the topographical peak (Figures 6b and 6e). At FLUX5 (south flank), the declination peaks west of the topographical high (Figures 6c and 6f) in the flank simulation, model, and direct measurements. Meyer and de Groot (2024) stated that the offset was not present at every site, and that it did not correlate with the orientation of the gully or the orientation with respect to the summit of Mt. Etna. We show here that this behavior is consistent with our flank simulations and represents an intrinsic feature of the MTE.

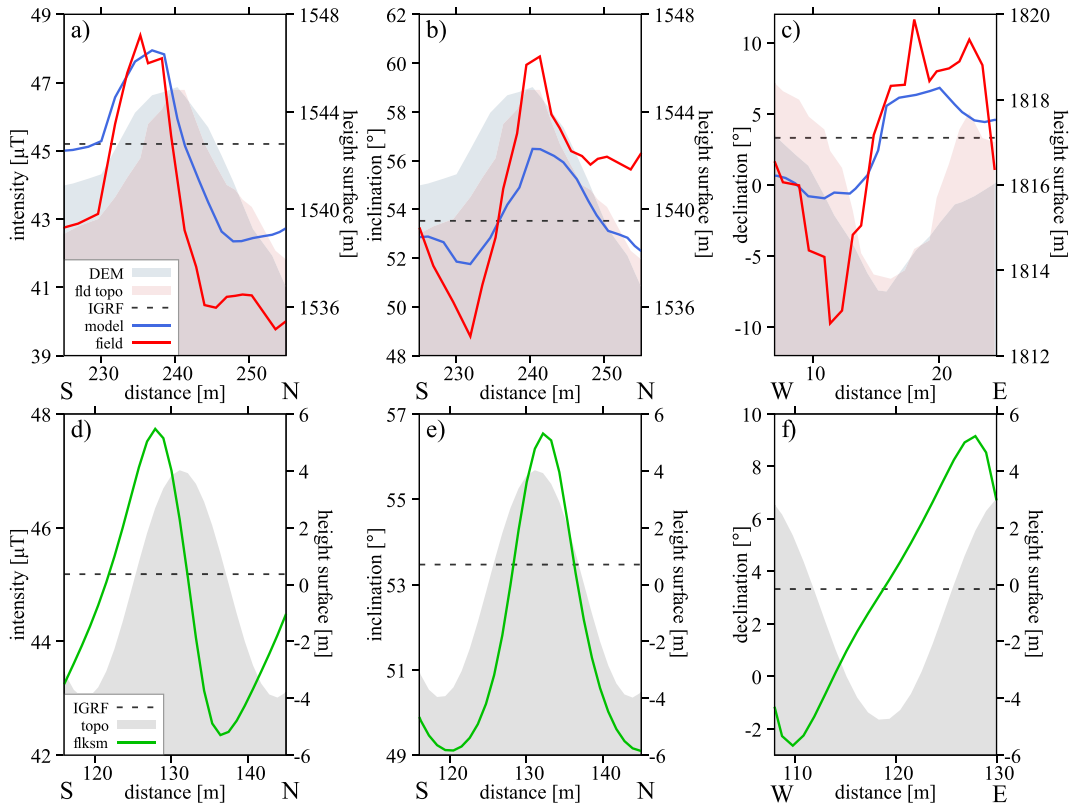


Figure 6. Comparison of "misaligned" peaks between direct measurements, model values and flank simulations, showing consistent trends. Segments from FLUX6 (a, b) show a south-shifted intensity and a north-shifted inclination peak, while the eastern flank simulation (flksm) results (d, e) show similar behavior. A segment from FLUX5, path 3 (c), shows a west-shifted declination peak, also observed in the southern flank simulations (f). Panels (a, b, d, and e) show results at 1 m height, whereas (c and f) are at 0.25 m, requiring an increased spatial resolution of 1000 × 1000 elements for the flank simulations.

Furthermore, the results from our flank simulations also explain the correlation trends identified by Meyer and de Groot (2024): inclination showed the strongest correlation between anomalies and topography, closely followed by intensity, whereas declination showed no such correlation. Two characteristics of the spatial misalignment between anomalies and the topography are important here. First, the magnitude of the spatial misalignment between the anomaly and topography peaks is largest for declination, smaller for intensity, and smallest for inclination. Second, the spatial misalignment is only present on specific flanks, depending on the magnetic field component. In our flank simulations (Figure 3), we observe that for declination anomalies the spatial misalignment is present on the north, east, and south flanks, whereas the intensity and inclination anomalies only misalign on the east and west flanks. The FLUX sites were located on the north, south, and east flanks of Mt. Etna. Consequently, declination is expected to be misaligned at all FLUX sites, while inclination and intensity anomaly peaks will only deviate from topographical highs at FLUX sites on the eastern flank (two out of the five FLUX sites included in the correlation analysis). The combination of offset magnitude and flank-dependent occurrence explains the statistical relationships identified by Meyer and de Groot (2024). The smaller and not consistently present spatial misalignment for intensity and inclination allows these anomalies to remain largely aligned with topography at most sites, producing the observed strong correlation. In contrast, the stronger misalignment of declination across all sampled flanks results in the weak observed correlation. This indicates that the lack of correlation between declination anomalies and topography does not imply the absence of MTEs in declination, but rather reflects the larger spatial offset between the anomaly and topographical feature driving it.

Lastly, we would like to reiterate that even though we emphasize the importance of volcanic flanks in MTE anomalies, we do not imply that these anomalies are generated by the entire volcanic mass, but rather by the slope present on each respective flank. This aligns with Tanguy and Le Goff (2004)'s findings, where the volcanic mass of Mt. Etna was found to not impact paleomagnetic measurements.

15252027, 2026, 10, Downloaded from https://agupubs.onlinelibrary.wiley.com/doi/10.1029/2026GC013098, Wiley Online Library on [07/11/2026]. See the Terms and Conditions (https://onlinelibrary.wiley.com/terms-and-conditions) on Wiley Online Library for rules of use; OA articles are governed by the applicable Creative Commons License

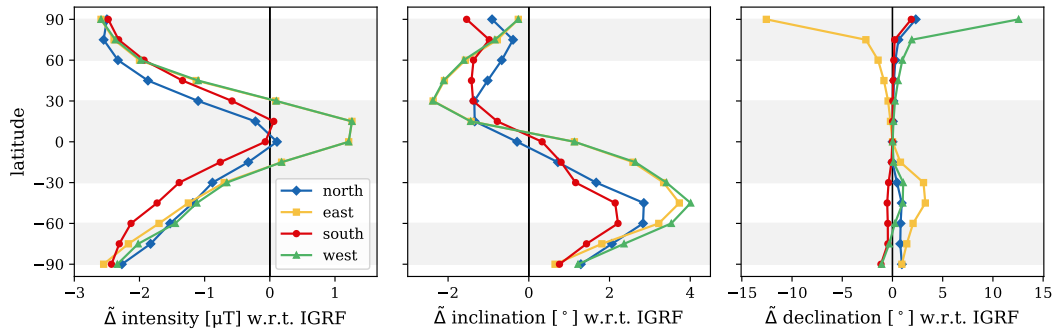


Figure 7. Median differences w.r.t. the IGRF $\left(\tilde{\Delta}\right)$ of intensity, inclination and declination for flank simulations at different latitudes using an Etna-like topography, showing an estimate of systematic bias. For each flank simulation run, the anomaly was computed at each point 1 m above the surface (see Section 2.3.1 for complete setup), after which the IGRF field values were added and the intensity, inclination and declination were computed. Next, the median of all measurement points on the flank was computed, and the IGRF intensity, inclination and declination were subtracted before plotting, thereby providing an estimate of the possible global MTE bias.

4.3. Global Variations

To evaluate the global implications of our findings, we applied Mt. Etna's flank simulations across a full range of latitudes, effectively "moving" the same topography from the geographic North Pole to the South Pole while recalculating the predicted MTEs as a function of latitude (Figure 7). These simulations were done by varying the inclination and intensity of the magnetization as a function of latitude, assuming a GAD. The magnetization at Mt. Etna, 7.5 A m^{-1}, was used as a reference value to scale the magnetization intensity at other latitudes using GAD latitude dependence. The IGRF-13 reference values were determined at an elevation of 1,300 m, at the same longitude as Mt. Etna (14.955°E), and on the first of April 2018.

One observed and anticipated trend is a positive inclination bias in the southern hemisphere. Such a persisting positive inclination anomaly from volcanic sources in the southern hemisphere has already been documented a few times: an inclination anomaly of 5° in Chile, 2° in Réunion Island and Antarctica (Biasi et al., 2021; Roperch et al., 2015; Tanguy et al., 2011). These values align well with our predictions. Additionally, declination anomalies in the southern hemisphere exhibit larger variations on all flanks, suggesting that an MTE bias in declination may persist even if all flanks are sampled well, although these deviations in the southern hemisphere may be explained by the presence of the South Atlantic Anomaly in the IGRF-13 reference data. Nevertheless, these findings are crucial given the growing focus on paleomagnetic research in the southern hemisphere due to a historical lack of data and the presence of the South Atlantic Anomaly. Lastly, our results show that while MTE intensity bias is predominantly negative across most latitudes, it becomes near-zero or positive within ±30° of the equator.

It is important to note that these simulations are based on Etnean topography and magnetization strength as a representative case. A sensitivity analysis (see Figure S28 in Supporting Information S1) shows that variations in topography parameters affect predominantly the absolute magnitude of MTE bias: steeper slopes and greater relief produce larger anomalies, whereas gentler slopes and lower relief produce smaller anomalies. Nevertheless, the broader trends and direction of the bias remain largely unchanged. The magnitude of the MTE-induced bias therefore cannot be assumed to apply directly to other volcanic settings. Authentic topographies, often more irregular than our generalized flank models, can also produce even larger anomalies, as demonstrated in our case study.

4.4. Suggestions for Paleomagnetic Research

As shown before, the MTE can only be avoided above a flat surface, in line with Baag et al. (1995). In most, if not all, volcanic regions, however, flat surfaces are very rare and the topography of the underlying lava flow is typically unknown. As a result, the influence of MTE on an individual TRM measurement generally cannot be distinguished from PSV. Improved sampling strategies, such as those proposed by Meyer and de Groot (2024),

15252027, 2026, 10, Downloaded from https://agupubs.onlinelibrary.wiley.com/doi/10.1029/2026GC013098, Wiley Online Library on [07/11/2026]. See the Terms and Conditions (https://onlinelibrary.wiley.com/terms-and-conditions) on Wiley Online Library for rules of use; OA articles are governed by the applicable Creative Commons License

15252027, 2026, 10, Downloaded from https://agupubs.onlinelibrary.wiley.com/doi/10.1029/2026GC013098, Wiley Online Library on [07/11/2026]. See the Terms and Conditions (https://onlinelibrary.wiley.com/terms-and-conditions) on Wiley Online Library for rules of use; OA articles are governed by the applicable Creative Commons License

can reduce some local effects, but completely eliminating systematic bias, particularly in inclination and intensity, remains difficult.

Nevertheless, the extent to which MTEs can be estimated and corrected depends on the available information. Lava flows frequently mantle pre-existing relief, and broad topographic characteristics may be inherited between successive flows or remain similar through time (Kilburn, 1996). MTEs above present-day topography or representative topography may thus provide a first-order estimate of past MTE bias. However, our results also show that small-scale topographic features, such as the crack-like feature at FLUX6, can generate large anomalies and are rarely resolved by DEMs, limiting this approach at the scale of individual measurements. The MTE model is therefore most useful for estimating systematic bias in sufficiently spatially and temporally distributed data sets, where small-scale local MTEs are reduced through averaging, and for assessing biases associated with a particular volcanic setting or sampling geometry, for example, if sampling was restricted to one flank. These estimates can be improved by adapting the synthetic topography model using local slope and lava-flow morphology, or by using a high-resolution DEM where available. We recommend that studies in rugged volcanic terrain include a detailed analysis of the local topography to estimate potential MTE contributions.

In light of these limitations, it is essential to reconsider our approach to volcanic paleomagnetic records. Although lava flows have long been regarded as reliable paleomagnetic recorders, our findings suggest they are subject to systematic biases introduced by MTE, in a way analogous to the inclination shallowing known from sedimentary records. Recognizing the presence of these biases and developing methods to correct for them are crucial steps for future paleomagnetic research. Additionally, we emphasize the importance of data sharing: providing detailed descriptions of sampling strategies and methodologies will improve the interpretability of published data sets and support the identification of possible MTE-related bias.

Finally, beyond its paleomagnetic applications, the MTE code presented here can also be used to compute the effect of topography on other magnetic data, including ground-based, drone-based, and shipborne magnetic surveys over rugged, strongly magnetized terrain.

5. Conclusion

This study highlights the critical importance of accounting for local terrain-induced magnetic anomalies in lava flows, particularly in regions characterized by strongly magnetized lava and rugged topography, where the potential for terrain-induced systematic bias in paleomagnetic data is high. Based on our findings, we conclude the following:

1. The model presented in this study can simulate realistic topographies and accurately compute the magnetic field above highly magnetized matter.
2. The model presented here can replicate field sites and paths using DEMs, and the computed values match the direct measurements to a high degree.
3. In areas of highly magnetized rock, such as lava flows, the topography of the underlying flow produces local magnetic anomalies in the magnetic field above the flow. The dispersion of the magnetic field components can be up to 20 % in magnitude and 21° in direction. These anomalies can be incorporated into future lava flows cooling on top, and therefore the MTE can have a significant impact on paleomagnetic research.
4. MTE anomalies do not occur above flat lava flows.
5. As discrimination between PSV and MTE in measured TRM data of lava flows is most often impossible in samples from volcanic terrain, the best method of acquiring accurate TRM data is by measuring at multiple sites far apart within the same lava flow, although a persistent systematic bias may still be present.
6. Incorporation of MTE into paleomagnetic data explains both local anomalies and systematic biases documented on Mt. Etna and across the northern hemisphere.
7. The impact of potential systematic bias due to MTEs in paleomagnetic records is globally variable, requiring a new approach focusing on recognition, quantification, and development of correction strategies to improve the reliability of paleomagnetic data from volcanic sources.

Conflict of Interest

The authors declare no conflicts of interest relevant to this study.

15252027, 2026, 10, Downloaded from https://agupubs.onlinelibrary.wiley.com/doi/10.1029/2026GC013098, Wiley Online Library on [07/11/2026]. See the Terms and Conditions (https://onlinelibrary.wiley.com/terms-and-conditions) on Wiley Online Library for rules of use; OA articles are governed by the applicable Creative Commons License

Availability Statement

The original FLUX data are available via Meyer and de Groot (2024)'s study. The direct measurements at the FLUX6 site were not included in the Yoda repository of Meyer and de Groot (2024), but are instead provided in a Zenodo repository (https://doi.org/10.5281/zenodo.21739781), which also hosts Version 2.1 of our MTE code used to produce the results of this study (Hendrickx & Thieulot, 2026). It includes all raw data (.ascii) files and plotting scripts required to reproduce the results presented here. The MTE code is also developed openly on GitHub (https://github.com/AgnesHendrickx/MTE). Furthermore, extensive documentation (a manual) of the code is available (https://mte.readthedocs.io/), including (plotting) scripts and instructions to reproduce key results in parameter testing, benchmarks and more. Due to copyright issues, the DEM snippets cannot be provided; however, sizes are listed in Table S1 in Supporting Information S1 to allow reproduction. Additionally, a detailed description of how to incorporate artificially generated DEMs is given in the code documentation.

Acknowledgments
This project has received funding from the Dutch Research Council (NWO) under its Talent program (VENI Grant 863.15.003 and VIDI Grant VI.Vidi.192.047 to LVdG). We thank Brendan Cych and an anonymous reviewer for their insightful comments.

References

Alken, P., Thébault, E., Beggan, C. D., Amit, H., Aubert, J., Baerenzung, J., et al. (2021). International geomagnetic reference field: The thirteenth generation. *Earth, Planets and Space*, *73*(1), 1–25. https://doi.org/10.1186/s40623-020-01288-x

Baag, C., Helsley, C. E., Xu, S.-Z., & Lienert, B. R. (1995). Deflection of paleomagnetic directions due to magnetization of the underlying terrain. *Journal of Geophysical Research*, *100*(B6), 10013–10027. https://doi.org/10.1029/95JB00148

Beck, M. E. (1984). Has the Washington-Oregon coast range moved northward? *Geology*, *12*(12), 737–740. https://doi.org/10.1130/0091-7613(1984)12<737:htwcrm>2.0.co;2

Biasi, J., Kirschvink, J. L., & Fu, R. R. (2021). Characterizing the geomagnetic field at high southern latitudes: Evidence from the antarctic peninsula. *Journal of Geophysical Research: Solid Earth*, *126*(12), e2021JB023273. https://doi.org/10.1029/2021JB023273

Biggin, A. J., Perrin, M., & Dekkers, M. J. (2007). A reliable absolute palaeointensity determination obtained from a non-ideal recorder. *Earth and Planetary Science Letters*, *257*(3), 545–563. https://doi.org/10.1016/j.epsl.2007.03.017

Bisson, M., Spinetti, C., Neri, M., & Bonforte, A. (2016). Mt. Etna volcano high-resolution topography: Airborne LiDAR modelling validated by GPS data. *International Journal of Digital Earth*, *9*(7), 710–732. https://doi.org/10.1080/17538947.2015.1119208

Blakely, R. J. (1995). *Potential theory in gravity and magnetic applications*. Cambridge University Press. https://doi.org/10.1017/CBO9780511549816.006

Bott, M. H. P. (1963). Two methods applicable to computers for evaluating magnetic anomalies due to finite three dimensional bodies. *Geophysical Prospecting*, *11*(3), 292–299. https://doi.org/10.1111/j.1365-2478.1963.tb02039.x

Branca, S., D'Ajello Caracciolo, F., Malaguti, A. B., & Speranza, F. (2019). Constraining age and volume of lava flow invasions of the Alcantara valley, Etna volcano (Italy). New insights from paleomagnetic dating and 3D magnetic modeling. *Journal of Volcanology and Geothermal Research*, *374*, 13–25. https://doi.org/10.1016/j.jvolgeores.2019.02.009

Castro, J., & Brown, L. (1987). Shallow paleomagnetic directions from historic lava flows, Hawaii. *Geophysical Research Letters*, *14*(12), 1203–1206. https://doi.org/10.1029/GL014i012p01203

Coe, R. S., Grommé, S., & Mankinen, E. A. (1978). Geomagnetic paleointensities from radiocarbon-dated lava flows on Hawaii and the question of the Pacific nondipole low. *Journal of Geophysical Research*, *83*(B4), 1740–1756. https://doi.org/10.1029/jb083ib04p01740

de Groot, B. M., & de Groot, L. V. (2019). A low-cost device for measuring local magnetic anomalies in volcanic terrain. *Geoscientific Instrumentation, Methods and Data Systems*, *8*(2), 217–225. https://doi.org/10.5194/gi-8-217-2019

de Groot, L. V., Mullender, T. A. T., & Dekkers, M. J. (2013). An evaluation of the influence of the experimental cooling rate along with other thermomagnetic effects to explain anomalously low palaeointensities obtained for historic lavas of Mt Etna (Italy). *Geophysical Journal International*, *193*(3), 1198–1215. https://doi.org/10.1093/gji/ggt065

Del Negro, C., & Ferrucci, F. (1998). Magnetic history of a dyke on Mount Etna (Sicily). *Geophysical Journal International*, *133*(2), 451–458. https://doi.org/10.1046/j.1365-246X.1998.00517.x

Di Mauro, D., Regi, M., Lepidi, S., Del Corpo, A., Dominici, G., Bagiacchi, P., et al. (2021). Geomagnetic activity at Lampedusa Island: Characterization and comparison with the other Italian observatories, also in response to space weather events. *Remote Sensing*, *13*(16), 3111. https://doi.org/10.3390/rs13163111

Griffiths, D. J. (2013). *Introduction to electrodynamics* (4th ed.). Pearson. Retrieved from https://cds.cern.ch/record/1492149

Hendrickx, A. E., & Thieulot, C. (2026). Mte v2.1 [Dataset]. *Zenodo*. https://doi.org/10.5281/zenodo.21739781

Herrero-Bervera, E., & Valet, J.-P. (2009). Testing determinations of absolute paleointensity from the 1955 and 1960 Hawaiian flows. *Earth and Planetary Science Letters*, *287*(3), 420–433. https://doi.org/10.1016/j.epsl.2009.08.035

Hill, M. J., & Shaw, J. (1999). Palaeointensity results for historic lavas from Mt Etna using microwave demagnetization/remagnetization in a modified Thellier-type experiment. *Geophysical Journal International*, *139*(2), 583–590. https://doi.org/10.1046/j.1365-246x.1999.00980.x

Jackson, J. D. (1999). *Classical electrodynamics* (3rd ed.). Wiley. Retrieved from http://cdsweb.cern.ch/record/490457

Kilburn, C. R. J. (1996). Patterns and predictability in the emplacement of subaerial lava flows and flow fields. In R. Scarpa & R. I. Tilling (Eds.), *Monitoring and mitigation of volcano hazards* (pp. 491–537). Springer. https://doi.org/10.1007/978-3-642-80087-0_15

Kilburn, C. R. J., & Lopes, R. M. C. (1988). The growth of AA lava flow fields on Mount Etna, sicily. *Journal of Geophysical Research*, *93*(B12), 14759–14772. https://doi.org/10.1029/JB093iB12p14759

Knudsen, M. F., Jacobsen, B. H., & Abrahamsen, N. (2003). Palaeomagnetic distortion modelling and possible recovery by inversion. *Physics of the Earth and Planetary Interiors*, *135*(1), 55–73. https://doi.org/10.1016/S0031-9201(02)00203-0

Magli, A., Speranza, F., Branca, S., Corsaro, R. A., Coltelli, M., Malaguti, A. B., & Giordano, G. (2024). Testing paleomagnetic dating on prehistoric flank eruptions from SE slope of Etna Volcano. *Journal of Geophysical Research: Solid Earth*, *129*(9), e2023JB028314. https://doi.org/10.1029/2023JB028314

Mahgoub, A. N., Reyes-Guzmán, N., Böhnel, H., Siebe, C., Pereira, G., & Dorison, A. (2018). Paleomagnetic constraints on the ages of the Holocene Malpaís de Zacapu lava flow eruptions, Michoacán (México): Implications for archeology and volcanic hazards. *The Holocene*, *28*(2), 229–245. https://doi.org/10.1177/0959683617721323

Meyer, R., & de Groot, L. V. (2024). Local magnetic anomalies explain bias in paleomagnetic data: Consequences for sampling. *Geochemistry, Geophysics, Geosystems*, *25*(5), e2023GC011319. https://doi.org/10.1029/2023GC011319

Mochizuki, N., Tsunakawa, H., Oishi, Y., Wakai, S., ichi Wakabayashi, K., & Yamamoto, Y. (2004). Palaeointensity study of the Oshima 1986 lava in Japan: Implications for the reliability of the Thellier and LTD-DHT Shaw methods. *Physics of the Earth and Planetary Interiors*, *146*(3), 395–416. https://doi.org/10.1016/j.pepi.2004.02.007

Nicolosi, I., Caracciolo, F. D., Branca, S., Ventura, G., & Chiappini, M. (2014). Volcanic conduit migration over a basement landslide at Mount Etna (Italy). *Scientific Reports*, *4*(1), 5293. https://doi.org/10.1038/srep05293

Nyblade, A. P., Shive, P. N., & Furlong, K. P. (1987). Rapid secular variation recorded in thick Eocene flows from the Absaroka Mountains of northwest Wyoming. *Earth and Planetary Science Letters*, *81*(4), 419–424. https://doi.org/10.1016/0012-821x(87)90128-2

Pavón-Carrasco, F. J., Tema, E., Osete, M. L., & Lanza, R. (2016). Statistical analysis of palaeomagnetic data from the last four centuries: Evidence of systematic inclination shallowing in lava flow records. *Pure and Applied Geophysics*, *173*(3), 839–848. https://doi.org/10.1007/s00024-014-0946-0

Reitz, J. R., & Milford, F. J. (1967). *Foundations of electromagnetic theory* (2nd ed. ed.). Addison-Wesley.

Ren, Z., Chen, C., Tang, J., Chen, H., Hu, S., Zhou, C., & Xiao, X. (2017). Closed-form formula of magnetic gradient tensor for a homogeneous polyhedral magnetic target: A tetrahedral grid example. *Geophysics*, *82*(6), WB21–WB28. https://doi.org/10.1190/geo2016-0470.1

Ren, Z., Chen, H., Chen, C., Zhong, Y., & Tang, J. (2019). New analytical expression of the magnetic gradient tensor for homogeneous polyhedrons. *Geophysics*, *84*(3), A31–A35. https://doi.org/10.1190/geo2018-0741.1

Ren, Z., Zhang, Y., Zhong, Y., Pan, K., Wu, Q., & Tang, J. (2022). Magnetic anomalies caused by 3D polyhedral structures with arbitrary polynomial magnetization. *Geophysical Research Letters*, *49*(18), e2022GL099209. https://doi.org/10.1029/2022GL099209

Roperch, P., Chauvin, A., Lara, L. E., & Moreno, H. (2015). Secular variation of the Earth's magnetic field and application to paleomagnetic dating of historical lava flows in Chile. *Physics of the Earth and Planetary Interiors*, *242*, 65–78. https://doi.org/10.1016/j.pepi.2015.03.005

Sherrod, D. R., Hagstrum, J. T., McGeehin, J. P., Champion, D. E., & Trusdell, F. A. (2006). Distribution, ^{14}C chronology, and paleomagnetism of latest Pleistocene and Holocene lava flows at Haleakalā volcano, Island of Maui, Hawai'i: A revision of lava flow hazard zones. *Journal of Geophysical Research*, *111*(B5), B05205. https://doi.org/10.1029/2005JB003876

Siciliana, R. (2010). Modello digitale del terreno (MDT) 2m x 2m Regione Siciliana-ATA 2007–2008 [Dataset]. Retrieved from http://www.sitr.regione.sicilia.it

Speranza, F., Branca, S., Coltelli, M., D'Ajello Caracciolo, F., & Vigliotti, L. (2006). How accurate is "paleomagnetic dating"? New evidence from historical lavas from Mount Etna. *Journal of Geophysical Research*, *111*(B12), B12S33. https://doi.org/10.1029/2006jb004496

Tanguy, J.-C., Bachèlery, P., & LeGoff, M. (2011). Archeomagnetism of Piton de la Fournaise: Bearing on volcanic activity at La Réunion Island and geomagnetic secular variation in Southern Indian Ocean. *Earth and Planetary Science Letters*, *303*(3), 361–368. https://doi.org/10.1016/j.epsl.2011.01.019

Tanguy, J.-C., & Le Goff, M. (2004). Distortion of the geomagnetic field in volcanic terrains: An experimental study of the Mount Etna stratovolcano. *Physics of the Earth and Planetary Interiors*, *141*(1), 59–70. https://doi.org/10.1016/j.pepi.2003.10.003

Tate, N. J., Brunsdon, C., Charlton, M., Fotheringham, A. S., & Jarvis, C. H. (2005). Smoothing/filtering LiDAR digital surface models. Experiments with loess regression and discrete wavelets. *Journal of Geographical Systems*, *7*(3), 273–290. https://doi.org/10.1007/s10109-005-0007-4

Tauxe, L. (2010). *Essentials of paleomagnetism*. University of California Press.

Torsvik, T. H., Van der Voo, R., Preeden, U., Mac Niocaill, C., Steinberger, B., Doubrovine, P. V., et al. (2012). Phanerozoic polar wander, palaeogeography and dynamics. *Earth-Science Reviews*, *114*(3), 325–368. https://doi.org/10.1016/j.earscirev.2012.06.007

Urrutia-Fucugauchi, J., Alva-Valdivia, L. M., Goguitchaichvili, A., Rivas, M. L., & Morales, J. (2004). Palaeomagnetic, rock-magnetic and microscopy studies of historic lava flows from the Paricutin volcano, Mexico: Implications for the deflection of palaeomagnetic directions. *Geophysical Journal International*, *156*(3), 431–442. https://doi.org/10.1111/j.1365-246X.2004.02166.x

Valet, J.-P., & Soler, V. (1999). Magnetic anomalies of lava fields in the Canary islands. Possible consequences for paleomagnetic records. *Physics of the Earth and Planetary Interiors*, *115*(2), 109–118. https://doi.org/10.1016/S0031-9201(99)00071-0

van Grinsven, L., Béguin, A., Kuiper, K. F., & de Groot, L. V. (2025). The evolution of a Mid-Miocene geomagnetic reversal. *Earth and Planetary Science Letters*, *667*, 119464. https://doi.org/10.1016/j.epsl.2025.119464

15252027, 2026, 10, Downloaded from https://agupubs.onlinelibrary.wiley.com/doi/10.1029/2026GC013098, Wiley Online Library on [07/11/2026]. See the Terms and Conditions (https://onlinelibrary.wiley.com/terms-and-conditions) on Wiley Online Library for rules of use; OA articles are governed by the applicable Creative Commons License